

Development of a Highly Potent, Novel M₅ Positive Allosteric Modulator (PAM) Demonstrating CNS Exposure: 1-((1*H*-Indazol-5-yl)sulfonyl)-*N*-ethyl-*N*-(2-(trifluoromethyl)benzyl)piperidine-4-carboxamide (ML380)

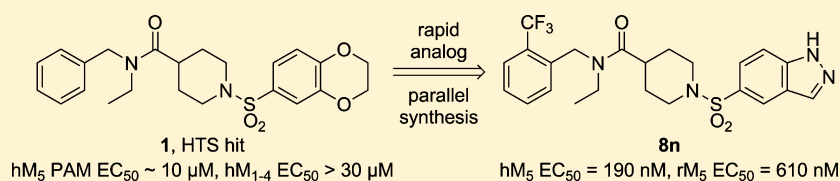
Patrick R. Gentry,^{†,‡,§} Masaya Kokubo,^{†,‡,§} Thomas M. Bridges,^{†,‡,§} Meredith J. Noetzel,^{†,‡,§} Hyekyung P. Cho,^{†,‡,§} Atin Lamsal,^{†,‡} Emery Smith,[‡] Peter Chase,[‡] Peter S. Hodder,[‡] Colleen M. Niswender,^{†,‡,§} J. Scott Daniels,^{†,‡,§} P. Jeffrey Conn,^{†,‡,§} Craig W. Lindsley,^{†,‡,||,§} and Michael R. Wood^{*,†,‡,||,§}

[†]Department of Pharmacology, [‡]Vanderbilt Center for Neuroscience Drug Discovery, and [§]Vanderbilt Specialized Chemistry Center for Accelerated Probe Development (MLPCN), Vanderbilt University Medical Center, Nashville, Tennessee 37232, United States

^{||}Department of Chemistry, Vanderbilt University, Nashville, Tennessee 37232, United States

[‡]Lead Identification Division, Molecular Screening Center, and Translational Research Institute, The Scripps Research Institute, 130 Scripps Way, Jupiter, Florida 33458, United States

Supporting Information



ABSTRACT: A functional high throughput screen identified a novel chemotype for the positive allosteric modulation (PAM) of the muscarinic acetylcholine receptor (mAChR) subtype 5 (M₅). Application of rapid analog, iterative parallel synthesis efficiently optimized M₅ potency to arrive at the most potent M₅ PAMs prepared to date and provided tool compound **8n** (ML380) demonstrating modest CNS penetration (human M₅ EC₅₀ = 190 nM, rat M₅ EC₅₀ = 610 nM, brain to plasma ratio (K_p) of 0.36).

INTRODUCTION

As a vital neurotransmitter, acetylcholine (ACh) activates ion channels and G protein coupled receptors (GPCRs) through its interactions with nicotinic and muscarinic (mAChR) acetylcholine receptors, respectively.^{1,2} Among the five mAChRs, subtypes 1, 4, and 5 (M₁, M₄, and M₅) are most strongly associated with normal central nervous system (CNS) functioning.² The M₂ and M₃ subtypes are more broadly expressed in the periphery on smooth muscle and glandular tissues³ such that aberrant overactivation of these receptors leads to the adverse effects associated with nonselective muscarinic agonists. Designing orthosteric small-molecule muscarinic ligands with sufficient selectivity over the other four mAChRs has long been a problem due to the highly conserved environment of the ACh binding site (the orthosteric site). A prudent response to instances such as this has been to abandon orthosteric-acting molecules in favor of ligands that interact at allosteric sites (sites that are topographically and structurally distinct from the endogenous agonist binding site).^{4,5} We have employed this approach to identify a range of high quality muscarinic ligands with positive allosteric modulation (PAM) or negative allosteric modulation

(NAM) at many of the CNS-important mAChRs: M₁ PAMs,⁶ M₄ PAMs,⁷ M₅ PAMs,⁸ and a novel M₅ NAM.⁹

Currently, M₅ is the least characterized of the mAChRs because of its low expression level¹⁴ and until recently an absence of selective activators and inhibitors. Nevertheless, phenotypic observations of M₅ knockout (KO) mice,³ M₅ receptor localization studies, and experiments utilizing non-selective, orthosteric muscarinic ligands highlight this receptor's therapeutic potential.² M₅ KO mice display decreased prepulse inhibition (a model of psychosis)¹⁰ and cognitive deficits associated with CNS neuronal and cerebrovascular abnormalities.¹¹ The loss of M₅ mAChRs in KO mice prevents their CNS vasculature from dilating in response to ACh,¹² which could have implications for cerebral hypoperfusion as related to Alzheimer's disease,¹³ schizophrenia, ischemic stroke, and migraine. Collectively, these data support the role of a M₅ PAM in the treatment of numerous CNS diseases. Here we report the development of the first CNS penetrant M₅ PAM,

Received: July 2, 2014

Published: August 22, 2014

which is structurally distinct from our previously reported isatin-containing M_5 PAMs.⁸

RESULTS AND DISCUSSION

High-Throughput Screen. Our initial foray into M_5 PAMs began with the identification of a nonselective M_1 , M_3 , M_5 PAM as a confirmed hit from an M_1 -focused high throughput screening (HTS) campaign.⁶ Although very high levels of M_5 selectivity were engendered through a strategically placed substituent on the isatin core, we were unable to detect these M_5 PAMs in rodent CNS. As such, we performed a high throughput screen directly interrogating M_5 functional activity in conjunction with the Scripps Research Institute Molecular Screening Center (SRIMSC). For this campaign, we used a triple addition protocol (compound addition followed by low and high concentrations of orthosteric agonist (ACh)) to screen the MLPCN¹⁴ collection of ~360 000 compounds. This screening strategy allows for the identification of activators (agonists and PAMs) while also surveying for inhibitors (NAMs and antagonists). Single concentration-point screening experiments in Chinese hamster ovary (CHO) cells stably expressing the human M_1 , M_4 , and M_5 receptors identified 3920 M_5 hits (1.07% hit rate). Hits were triaged based on activity in untransfected cells, structural tractability, and the elimination of frequent hitters.¹⁵ The most attractive M_5 activators were purchased from commercial sources and reconfirmed using 10-point concentration–response curves (CRC). These “triple-add” CRC experiments resulted in the identification of nine confirmed M_5 PAMs, nine M_5 antagonists,^{9,16} and zero M_5 agonists.

Chemistry. Structurally, the most promising of the M_5 PAM hits, **1** (Figure 1), represented a novel chemotype for an M_5

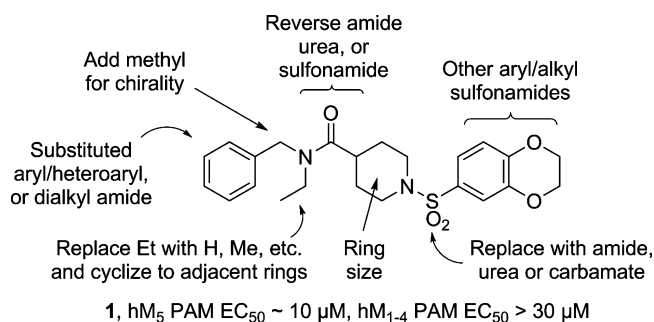
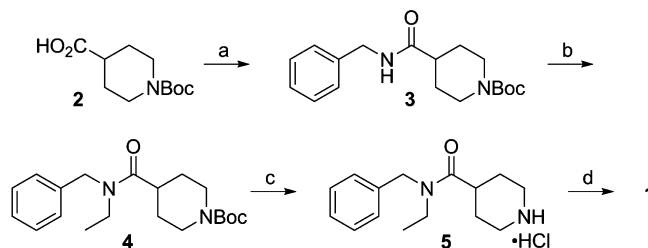


Figure 1. Structure and initial plans to modify HTS hit **1**.

PAM and offered a wide range of straightforward modifications due to its highly modular appearance. The broad range of planned modifications to **1**, shown in Figure 1, could readily be accomplished by employing the synthesis route shown in Scheme 1. Starting from the *N*-Boc protected carboxylic acid core **2**, peptide coupling with an amine introduced the first alkyl group on amide **3**. Deprotonation of this amide was followed by the addition of an alkylating agent (e.g., ethyl iodide) and a crown ether, necessary to facilitate the introduction of the second alkyl group, providing **4**. Removal of the Boc protecting group under standard anhydrous HCl conditions provided the salt **5**. The amine of **5** was then sulfonylated to provide the HTS hit **1**. Alternatively, this secondary amine could be functionalized through reactions with a wide range of electrophiles (e.g., acid chlorides, isocyanates, alkyl halides, etc.). Although the synthesis route

Scheme 1. Synthesis of M_5 PAM HTS Hit **1** and Its Analogs^a



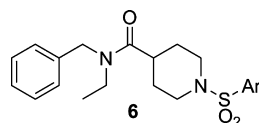
^aReagents and conditions: (a) benzylamine, HATU, DCM, DIPEA, 95%; (b) NaOtBu, Et-I, 15-crown-5, THF, 88%; (c) HCl, dioxane, 99%; (d) 1,4-benzodioxan-6-sulfonyl chloride, DCM, DIPEA, 70%.

was quite flexible, when applied to many of the modifications proposed in Figure 1, the SAR was disappointingly rigid. A litany of modifications were not tolerated and resulted in a complete loss of M_5 activity: (1) removal of *N*-benzyl or *N*-ethyl moiety to provide a secondary amide, (2) cyclizing the ethyl group back to the piperidine, (3) relocating the carbonyl to produce the acetamide or benzamide analogs, (4) replacing the amide with a sulfonamide, (5) replacing the piperidine with an azetidine or [1.3.0] bicycle, (6) replacing the sulfonamide with an amide, urea, or carbamate, and (7) any alkylsulfonamide in place of an arylsulfonamide. The failure of these global modifications suggested that an improvement in potency would require a better understanding of the M_5 PAM SAR brought about by more modest modifications.

Initial improvements in PAM potency were provided by modifications to the arylsulfonamide (Table 1). The unadorned phenylsulfonamide **6a** showed slightly improved potency over the HTS hit; however, potency could be further improved through the introduction of methoxy groups at the para and meta positions. Interestingly, the 3,4-dimethoxy analog **6e** displayed slightly reduced efficacy (ACh_{max}) relative to the HTS hit and may speak to the preference for sulfonamides with more planar aryl groups at this location. Substitution at the ortho position was clearly disfavored as indicated by **6d** and the sulfonamide regioisomer of the HTS hit **6f**. A sampling of alternative monocyclic heteroaryl groups (**6g–m**) did not provide improved activity. Building on the importance of substituents at the 3 and 4 positions, we explored a range of bicyclic heteroarylsulfonamides with annulated rings spanning these two positions. A number of heterocycles showed significant improvements over the HTS hit. In particular, the benzofuranyl (**6o**) and indazolylsulfonamides (**6p** and **6q**) provided hM_5 PAMs with EC_{50} of 1.6–2.4 μM , representing an approximately 3-fold improvement over the naked phenylsulfonamide.

Employing sulfonamides structurally related to those appearing in Table 1, we explored changes to the western region of **1** and were gratified that introduction of a methyl group at the benzylic position improved potency while demonstrating enantiospecific activity (Table 2). While the (*S*)-enantiomer **7a** was inactive at hM_5 , the (*R*)-methyl enantiomer **7b** demonstrated a 3-fold improvement in potency relative to its des-methyl analog **6b**. This improvement in potency was maintained across the benzofuranyl (**7c**) and 2,3-dihydrobenzofuranyl (**7d**) analogs. Although slight improvements in hM_5 PAM potency were realized with the incorporation of 2,3-dihydroindenyl and the 6- and 5-indazolylsulfonamides (**7e**, **7f**, and **7g**, respectively).

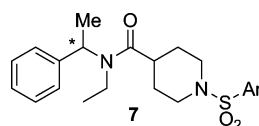
Table 1. Structures and Activities of Analogs 6



compd	Ar	hM ₅ pEC ₅₀ ^a	hM ₅ EC ₅₀ (μM)	ACh max ^a (%)
6a	phenyl	5.21 ± 0.06	6.2	69 ± 3
6b	4-methoxyphenyl	5.48 ± 0.06	3.3	84 ± 3
6c	3-methoxyphenyl	5.51 ± 0.09	3.1	77 ± 4
6d	2-methoxyphenyl	—	>10	—
6e	3,4-dimethoxyphenyl	<5	>10	57 ± 3
6f	2,3-dihydrobenzo[<i>b</i>][1,4]dioxin-5-yl	<5	>10	53 ± 2
6g	imidazol-4-yl	—	>10	—
6h	5-methylthiophen-2-yl	<5	>10	64 ± 3
6i	3,5-dimethylisoxazol-4-yl	—	>10	—
6j	6-(trifluoromethyl)pyridin-3-yl	—	>10	—
6k	pyridin-4-yl	—	>10	—
6l	pyridin-3-yl	—	>10	—
6m	pyridin-2-yl	—	>10	—
6n	quinolin-7-yl	<5	>10	66 ± 3
6o	benzofuran-5-yl	5.63 ± 0.11	2.4	80 ± 5
6p	1H-indazol-5-yl	5.81 ± 0.08	1.6	86 ± 4
6q	1H-indazol-6-yl	5.77 ± 0.09	1.7	86 ± 4
6r	benzo[<i>c</i>][1,2,5]thiadiazol-5-yl	5.53 ± 0.11	3.0	81 ± 5
6s	benzo[<i>c</i>][1,2,5]thiadiazol-4-yl	—	>10	—
6t	benzo[<i>d</i>][1,3]dioxol-5-yl	5.13 ± 0.16	7.4	93 ± 12

^ahM₅ pEC₅₀ and ACh max data reported as averages ± SEM from our calcium mobilization assay; *n* = 3–4 determinations; —, not determined.

Table 2. Structures and Activities of Analogs 7



compd	*	Ar	hM ₅ pEC ₅₀ ^a	hM ₅ EC ₅₀ (μM)	ACh max ^a (%)
7a	S	4-methoxyphenyl	—	inactive	—
7b	R	4-methoxyphenyl	6.01 ± 0.07	0.97	90 ± 3
7c	R	benzofuran-5-yl	6.03 ± 0.06	0.93	80 ± 2
7d	R	2,3-dihydrobenzofuran-5-yl	5.95 ± 0.05	1.11	88 ± 2
7e	R	2,3-dihydro-1H-inden-5-yl	6.14 ± 0.05	0.73	97 ± 2
7f	R	1H-indazol-6-yl	6.12 ± 0.05	0.76	87 ± 2
7g	R	1H-indazol-5-yl	6.13 ± 0.04	0.74	86 ± 1

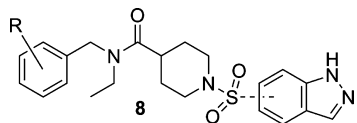
^ahM₅ pEC₅₀ and ACh max data reported as averages ± SEM from our functional calcium mobilization assay; *n* = 3–4 determinations; —, not determined.

Simultaneously, we were exploring modifications to the western aryl ring in the context of the indazole sulfonamides and identified a number of productive alterations depicted in Table 3. Systematically moving a fluorine around the phenyl ring revealed that substitution at the 2 and 3 positions was favored, with a trend in preference for the 3-fluoro **8b**. As such, small groups were introduced at the meta position. Most notably, the 3-methyl analog **8f** yielded a submicromolar potency (hM₅ EC₅₀ = 0.87 μM). This potency was mirrored by the analogous 2-methyl analog **8g** and prompted a further exploration of substituents at the ortho position. The 2-chloro (**8i**) and 2-trifluoromethyl (**8j**) groups provided further improvements in potency, but interestingly the 3- and 4-trifluoromethyl analogs (**8k** and **8l**, respectively) possessed greatly reduced activity and illustrated the frequently steep nature of allosteric SAR. The two most potent ortho-

substituted analogs (Cl and CF₃) with the 6-indazolyl-sulfonamide were also examined in the context of the 5-indazolylsulfonamide (**8m** and **8n**) and found to be among the most potent hM₅ PAMs prepared to date. Specifically, **8n**, displaying a hM₅ PAM EC₅₀ = 0.19 μM, was 8-fold more potent than its *des*-CF₃ congener (**6p**, Table 1). Disappointingly, addition of a methyl group in the (*R*) configuration to **8n**, analogous to the compounds in Table 2, resulted in a 10-fold decrease in potency (hM₅ EC₅₀ = 2.4 μM, structure not shown).

In vitro metabolite identification experiments performed on **7g** implicated the *N*-ethyl moiety as the primary site of metabolism. While we were simultaneously exploring modification to this *N*-ethyl group with variations at other locations, a concise but still representative description of these efforts can be summarized in the context of the highly optimized **8n** and

Table 3. Structures and Activities of Analogs 8

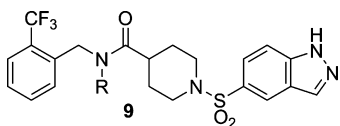


compd	R	indazolyl attachment	hM ₅ pEC ₅₀ ^a	hM ₅ EC ₅₀ (μM)	ACh max ^a (%)
8a	4-F	6	<5	>10	55 ± 3
8b	3-F	6	5.82 ± 0.04	1.5	89 ± 2
8c	2-F	6	5.67 ± 0.12	2.1	84 ± 5
8d	3-Cl	6	5.79 ± 0.06	1.6	77 ± 2
8e	3-MeO	6	5.58 ± 0.10	2.6	85 ± 5
8f	3-Me	6	6.06 ± 0.07	0.87	78 ± 2
8g	2-Me	6	6.06 ± 0.07	0.87	103 ± 3
8h	2-MeO	6	6.12 ± 0.06	0.75	92 ± 3
8i	2-Cl	6	6.19 ± 0.05	0.64	93 ± 2
8j	2-CF ₃	6	6.32 ± 0.04	0.48	92 ± 2
8k	3-CF ₃	6	5.26 ± 0.09	5.6	59 ± 3
8l	4-CF ₃	6	—	inactive	—
8m	2-Cl	5	6.46 ± 0.08	0.35	78 ± 2
8n	2-CF ₃	5	6.71 ± 0.06	0.19	96 ± 2

^ahM₅ pEC₅₀ and ACh max data reported as averages ± SEM from our calcium mobilization assay; *n* = 3–5 determinations; —, not determined.

its analogs appearing in Table 4. Although not bearing the optimized 5-indazolesulfonamide shown in Table 4, early

Table 4. Structures and Activities of Analogs 9



compd	R	hM ₅ pEC ₅₀ ^a	hM ₅ EC ₅₀ (μM)	ACh max ^a (%)
9a	<i>n</i> -propyl	6.81 ± 0.06	0.16	94 ± 2
9b	allyl	5.74 ± 0.04	1.8	79 ± 2
9c	isopropyl	<5	>10	54 ± 3
9d	cyclopropyl	—	inactive	—
9e	cyclobutyl	5.74 ± 0.09	1.8	84 ± 4
9f	2-hydroxyethyl	<5	>10	60 ± 3
9g	2-fluoroethyl	5.90 ± 0.07	1.3	95 ± 4
9h	<i>sec</i> -butyl	6.82 ± 0.06	0.15	100 ± 2
9i	neopentyl	6.91 ± 0.06	0.12	104 ± 2
9j	cyclopropylmethyl	6.92 ± 0.06	0.12	102 ± 2
9k	cyclobutylmethyl	6.89 ± 0.05	0.13	103 ± 2

^ahM₅ pEC₅₀ and ACh max data reported as averages ± SEM from our calcium mobilization assay; *n* = 3–5 determinations; —, not determined.

results indicated that groups smaller than ethyl (i.e., hydrogen or methyl) resulted in a complete loss of, or greatly diminished,

activity at hM₅ (respectively, structures not shown). The ethyl group in **8n** could be extended without incurring a loss in potency as demonstrated by the *n*-propyl analog **9a**. However, the other three-carbon isomers (**9b–d**) all suffered a >10-fold drop in activity. Attempts to mitigate metabolism through the introduction of polarity on the terminus of the ethyl group in **8n** similarly engendered an unacceptable decrease in activity upon introduction of a hydroxyl (**9f**) or even a single fluorine atom (**9g**). Given the complete absence of activity demonstrated by the cyclopropyl analog **9d**, it was surprising to find that the cyclobutyl version (**9e**) displayed mid-micromolar potency. Supporting the hypothesis that alkyl branching is not well tolerated directly adjacent to the amide nitrogen (i.e., **9c–e**) but that larger alkyl groups could be present more distally, the *sec*-butyl analog **9h** was equipotent to its *n*-propyl congener (**9a**). Furthermore, even larger alkyl groups at this location (**9i–k**) displayed consistently high levels of activity. Unfortunately, none of these modifications could shift the primary route of metabolism away from this region of these molecules while maintaining high levels of M₅ PAM activity, nor could they attenuate an inherently high rate of *in vitro* metabolism (i.e., rat hepatic microsomal CL_{int} > 500 mL min^{−1} kg^{−1}). However, **9d** was able to reduce intrinsic microsomal clearance by an order of magnitude, but this came at the expense of losing all hM₅ activity.

Pharmacology and Selectivity. A subset of M₅ PAMs were further assessed for their ability to enhance the potency of ACh at the hM₅ receptor using a fluorescence based calcium mobilization assay. Experimentally, a fixed concentration of PAM (10 μM) or vehicle was added prior to the addition of a concentration response curve (CRC) of ACh, and the left shift in potency of ACh was determined as the ratio (fold shift) of the potency in the absence and presence of PAM. As shown in Table 5, the HTS hit **1** produced a fold shift of 2.3, while the more potency-optimized analogs showed at least twice that value. Four of the most potent compounds from Tables 2 and 3 (**7b**, **7g**, **8j**, and **8n**) gave fold shift values in the 7- to 12-fold range, similar to earlier M₅ PAMs.⁸

Although **7g** and **8n** displayed similar fold shift values, **8n** was superior to **7g** with respect to hM₅ PAM potency and by virtue of its superior muscarinic subtype selectivity profile.¹⁷ The muscarinic subtype selectivity profile for **8n** across the five human and rat receptor subtypes can be seen in Figure 2. **8n** shows no activity at hM₂ or hM₄ (the natively G_{i/o} coupled mAChRs; our assays employed cells co-transfected with chimeric G_{q15} to facilitate M₂/M₄ coupling to Ca²⁺ mobilization) and displays greater than 10-fold selectivity over hM₁ and hM₃ (the G_q coupled mAChRs). The lower potencies, combined with lower efficacies, at hM₁ (hM₁ PAM EC₅₀ = 5.4 μM, ACh_{max} = 52%) and hM₃ (hM₃ PAM EC₅₀ = 2.1 μM, ACh_{max} = 67%) when compared to those for **8n** at hM₅ (hM₅ PAM EC₅₀ = 0.19 μM, ACh_{max} = 96%) may actually afford a greater than 10-fold selectivity window. Interestingly, when assessed at the rat muscarinic receptors, the level of

Table 5. ACh Fold-Shift Values for Select M₅ PAMs

	compd						
	1	6p	6q	7b	7g	8j	8n
ACh fold shift ^a	2.3 ± 0.1	5.4 ± 0.7	4.8 ± 0.4	7 ± 1	12 ± 3	7 ± 2	9 ± 4

^aACh fold-shift data, for compounds at 10 μM, reported as averages ± SEM from our calcium mobilization assay and represent leftward shifts in ACh potency; *n* = 3–4.

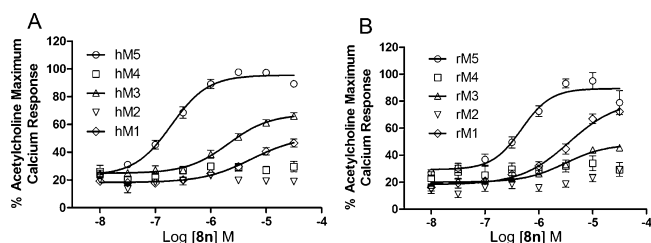


Figure 2. Muscarinic subtype selectivity profile of **8n**: (A) human selectivity (hM₅ EC₅₀ = 0.19 μ M, hM₄ EC₅₀ > 30 μ M, hM₃ EC₅₀ = 2.1 μ M, hM₂ EC₅₀ > 30 μ M, hM₁ EC₅₀ = 5.4 μ M); (B) rat selectivity (rM₅ EC₅₀ = 0.61 μ M, rM₄ EC₅₀ > 30 μ M, hM₃ EC₅₀ = 3.1 μ M, hM₂ EC₅₀ > 30 μ M, hM₁ EC₅₀ = 2.0 μ M). Data represent the mean \pm SEM from at least three independent determinations employing highly expressing cell lines with similarly high expression levels of muscarinic receptors.

subtype selectivity diminished and rM₁ was now closest in potency to rM₅.

The pharmacology of **8n** was further profiled in radioligand binding experiments (Figure 3). Increasing concentrations of

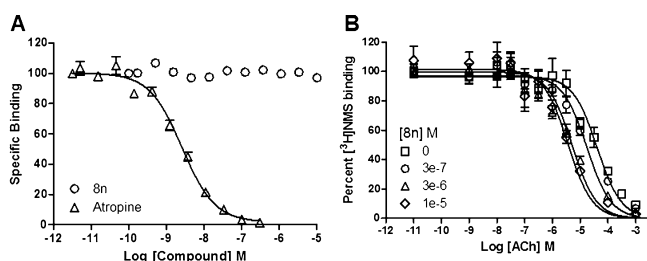


Figure 3. (A) [³H]NMS competition binding. **8n** has no inhibitory effect on [³H]NMS binding (97.1% max), while the control (atropine) inhibits [³H]NMS binding in a concentration dependent manner (K_i = 1.47 nM, 1.8% max). (B) Acetylcholine affinity shift profile of **8n**. Increasing fixed concentrations of **8n** result in progressive left shifts of the ACh inhibition curve, with a maximal shift of approximately 15. Experiments were performed using membranes prepared from hM₅ CHO cells. Data represent the mean \pm SEM from at least three independent determinations.

8n or atropine (control) were incubated with a fixed concentration of [³H]*N*-methylscopolamine (NMS, 0.3 nM, an orthosteric antagonist) and membranes expressing the hM₅ receptor. While atropine displaced [³H]NMS binding in a concentration dependent manner, **8n** had no effect on [³H]NMS binding (Figure 3A), suggesting that **8n** interacts with the hM₅ receptor via an allosteric mechanism. To further characterize the interaction of **8n** with the hM₅ receptor, increasing fixed concentrations of **8n** were incubated with a CRC of ACh in the presence of a fixed concentration of [³H]NMS (0.4 nM) to determine the effect of **8n** on the affinity of ACh. **8n** shifted the ACh competition curve leftward by ~15-fold (Figure 3B), further demonstrating its function as a PAM, acting through modulation of the potency and affinity of ACh. However, it has yet to be defined what in vitro properties are required for a hM₅ PAM to generate a specific in vivo outcome. Only now are we beginning to amass the necessary tool compounds to explore this question.

Interestingly, this novel class of hM₅ PAMs showed a clear preference for the G_q coupled mAChRs over the G_{i/o} coupled receptors, which is reminiscent of the nonselective pan-G_q PAM HTS hit⁸ that served as the progenitor for three previous M₅ PAM probe molecules⁸ and an M₁ selective PAM.⁶ This

similarity points to the possibility of a common allosteric binding site and the high probability that further SAR will reveal completely selective M₅ PAMs from this series. To more broadly explore this new scaffold's potential for nonmuscarinic, off-target activity, **8n** was submitted to Eurofin's Pan Labs lead profiling screen. This battery of radioligand binding assays consists of 68 common GPCRs, ion channels, and transporters where the test compound (**8n**) was present at 10 μ M. Remarkably, **8n** showed a significant response (>49% radioligand displacement; see Supporting Information for complete results) in just two assays: cannabinoid CB₁ receptor (50% displacement) and σ_1 receptor (53% displacement). However, these binding results do not guarantee functional activity and the mid-range values did not prompt functional determinations.

Metabolism and Disposition. Encouraged by these initial results, **8n** was characterized in a variety of DMPK assays (Table 6). From an in vitro standpoint, **8n** displayed minimal

Table 6. DMPK Profile of **8n**

	in vitro	in vivo
microsome CL _{int} (mL/min/kg)	rat: 2600	(male, Sprague–Dawley, <i>n</i> = 3)
	human: 540	CL _{plasma} (mL/min/kg) 66
predicted CL _{hep} ^a (mL/min/kg)	rat: 68	elimination <i>t</i> _{1/2} (min) 22
	human: 20	Vd _{ss} (L/kg) 1.6
<i>f</i> _u plasma	rat: 0.014	brain/plasma <i>K</i> _p 0.36
	human: 0.015	(at 15 min) <i>K</i> _{p,uu} 0.28
<i>f</i> _u brain	rat: 0.011	

^aDetermined using CL_{int} values in the well-stirred model of organ clearance not corrected for fraction unbound in plasma.

metabolic stability with a very high hepatic microsomal intrinsic clearance in rat and human (CL_{int}; rat, 2600 mL min⁻¹ kg⁻¹; human, 540 mL min⁻¹ kg⁻¹) and a correspondingly high predicted hepatic clearance in both species (CL_{hep}; rat, 68 mL min⁻¹ kg⁻¹; human, 20 mL min⁻¹ kg⁻¹), on par with hepatic blood flow. A low fraction unbound in plasma was observed for rat and human (*f*_{u,plasma}; rat, 0.014; human, 0.015) and in rat brain homogenate (*f*_{u,brain}; rat, 0.011). In rodents (male, Sprague–Dawley rats, 1 mg/kg iv, *n* = 3), similar instability was observed after intravenous dosing; **8n** displayed high clearance (66 mL min⁻¹ kg⁻¹), a moderate volume of distribution (1.6 L kg⁻¹), and a short half-life (*t*_{1/2}, 22 min). A modest total brain-plasma partition coefficient (*K*_p = 0.36) was also determined from these experiments (15 min after administration); however, the unbound brain-plasma partition coefficient (*K*_{p,uu} = 0.28) tempers the attractiveness of **8n** as a highly CNS penetrant compound. Still, the high permeability determined in Caco-2 cells (*P*_{app} = 2.5 \times 10⁻⁵ cm/s) represents an attractive starting point to further optimize CNS exposure.

CONCLUSION

In summary, we have developed **8n** (also referred to as ML380 or VU0481443), which is among the most potent M₅ PAMs reported to date (hM₅ EC₅₀ = 190 nM, rM₅ EC₅₀ = 610 nM) and is M₅ preferring with some functional activity remaining at M₁ and M₃. This compound will be a useful tool to further investigate the in vitro properties of the M₅ receptor as more advanced PAMs are identified. This novel chemotype distinguishes itself from our previously published isatin-containing M₅ PAMs in its ability to be detected within the CNS even though its partition coefficients (*K*_p and *K*_{p,uu}) are

less than optimal. However, the highly modular nature of this ligand will allow for continued structural optimization to further improve potency, selectivity, metabolic stability, and CNS penetration. Continuing efforts around this scaffold are in progress and will be reported in due course.

EXPERIMENTAL SECTION

Chemistry. The general chemistry, experimental information, and syntheses of key compounds are supplied in the Supporting Information. Purity for all final compounds was >95%, and each showed a parent mass ion consistent with the desired structure (LCMS).¹⁷

1-((1*H*-indazol-5-yl)sulfonyl)-*N*-ethyl-*N*-(2-(trifluoromethyl)-benzyl)piperidine-4-carboxamide (8n). To a solution of 1-Boc-4-piperidinecarboxylic acid (2.00 g, 8.72 mmol, 1 equiv) and DIPEA (4.48 mL, 26.2 mmol, 3 equiv) in DCM (30 mL, 0.3 M) was added 1-ethyl-3-(3-dimethylaminopropyl)carbodiimide HCl (2.51 g, 13.1 mmol, 1.5 equiv), hydroxybenzotriazole (1.77 g, 13.1 mmol, 1.5 equiv), and ethylamine HCl (1.42 g, 17.5 mmol, 2.0 equiv). The mixture was stirred for 2 h at room temperature before being quenched with aqueous NaHCO₃. The organic layer was separated, and the aqueous layer was extracted with DCM. The combined organic layers were washed with brine, dried over MgSO₄, filtered, and concentrated under reduced pressure. The residue was purified via silica gel column chromatography to give 1.89 g of 1-Boc-4-(ethylcarbamoyl)piperidine (83% yield). To a solution of 1-Boc-4-(ethylcarbamoyl)piperidine (50.0 mg, 0.195 mmol, 1 equiv) and 15-crown-5 (77.4 μ L, 0.390 mmol, 2 equiv) in THF (2 mL, 0.1 M) was added NaO^tBu (28.1 mg, 0.293 mmol, 1.5 equiv). The mixture was stirred for 30 min at room temperature before adding 2-(trifluoromethyl)benzyl bromide (59.4 μ L, 0.39 mmol, 2 equiv). After 16 h, the mixture was concentrated under reduced pressure and the residue partitioned between H₂O and DCM. The organic layer was separated, and the aqueous layer was extracted with DCM. The combined organic layers were concentrated under reduced pressure and the residue was purified via Gilson preparative LC (MeCN/water/0.1% TFA gradient as the mobile phase through a c-18 column) to obtain 1-Boc-4-(ethyl(2-(trifluoromethyl)benzyl)carbamoyl)piperidine. To a solution of 1-Boc-4-(ethyl(2-(trifluoromethyl)benzyl)carbamoyl)piperidine in DCM was added MP-TsOH (5 equiv). The mixture was heated to 100 °C under microwave irradiation for 10 min. The mixture was filtered, and the resin was rinsed with MeOH before washing with NH₃/MeOH to elute product. Solvent was removed under reduced pressure to give 43 mg of pure 4-(ethyl(2-(trifluoromethyl)benzyl)carbamoyl)piperidine (70% yield, two steps). To a solution of 4-(ethyl(2-(trifluoromethyl)benzyl)carbamoyl)piperidine (20 mg, 0.063 mmol, 1 equiv) and DIPEA (33 μ L, 0.20 mmol, 3 equiv) in DCM was added 1*H*-indazole-5-sulfonyl chloride (21 mg, 0.095 mmol, 1.5 equiv). The mixture was allowed to stir for 2 h at room temperature and was then quenched with MeOH and concentrated under reduced pressure. The residue was purified via Gilson preparative LC (MeCN/water/0.1% TFA gradient as the mobile phase through a c-18 column) to obtain 4.2 mg of **8n** (15% yield). HRMS (TOF, ES⁺) C₂₃H₂₆N₄O₃F₃S [M + H]⁺ calcd mass 495.1678, found 495.1679. ¹H NMR (1:1.25 rotamer ratio, * denotes minor rotamer, 400.1 MHz, CDCl₃) δ (ppm): 8.31 (s, 1H); 8.25 (m, 1H); 7.78, 7.72* (d, *J* = 8.8 Hz, 1H); 7.68–7.57 (m, 2H); 7.52*, 7.46 (t, *J* = 7.6 Hz, 1H); 7.38*, 7.32 (t, *J* = 7.6 Hz, 1H); 7.21–7.13 (m, 1H); 4.76, 4.64* (s, 2H); 3.95–3.86, 3.85–3.76* (m, 2H); 3.41*, 3.22 (q, *J* = 7.2 Hz, 2H); 2.60–2.46 (m, 2H); 2.37–2.26 (m, 1H); 2.11–1.92 (m, 2H); 1.91–1.81, 1.74–1.65* (m, 2H); 1.16–1.05 (m, 3H). ¹³C NMR (1:1.35 rotamer ratio, * denotes minor rotamer, 100.6 MHz, CDCl₃) δ (ppm): 174.70; 141.40, 141.34*; 136.29, 135.77*; 135.95; 132.67*, 132.31; 129.31*, 129.19; 127.94, 127.86*; 127.90 (q, *J* = 30.3 Hz); 126.65 (q, *J* = 5.3); 126.47; 126.26 (q, *J*_{CF} = 245 Hz); 126.04 (q, *J* = 5.6 Hz); 122.81, 122.73*; 122.66; 110.92, 110.89*; 46.94*, 44.23; 45.64, 45.46*; 42.12, 41.87*; 37.96*, 37.68; 28.48, 28.27*; 14.44, 12.67*.

ASSOCIATED CONTENT

Supporting Information

Experimental procedures and spectroscopic data for selected compounds, detailed pharmacology, and DMPK methods. This material is available free of charge via the Internet at <http://pubs.acs.org>.

AUTHOR INFORMATION

Corresponding Author

*Phone: 615-322-0670. Fax: 615-343-3088. E-mail: michael.r.wood@vanderbilt.edu.

Notes

The authors declare no competing financial interest.

ACKNOWLEDGMENTS

This work was generously supported by Grant NIH/MLPCN U54 MH084659 (C.W.L.) and Grant U54 MH084512 (Scripps).

ABBREVIATIONS USED

hM₅, human muscarinic acetylcholine receptor subtype 5; MLPCN, Molecular Libraries Probe Production Centers Network; NMS, *N*-methylscopolamine

REFERENCES

- (1) Smythies, J. Section I. The cholinergic system. *Int. Rev. Neurobiol.* **2005**, *64*, 1–122.
- (2) Dencker, D.; Thomsen, M.; Wortwein, G.; Weikop, P.; Cui, Y.; Jeon, J.; Wess, J.; Fink-Jensen, A. Muscarinic acetylcholine receptor subtypes as potential drug targets for the treatment of schizophrenia, drug abuse, and Parkinson's disease. *ACS Chem. Neurosci.* **2011**, *3*, 80–89.
- (3) Wess, J.; Eglen, R. M.; Gautam, D. Muscarinic acetylcholine receptors: mutant mice provide new insights for drug development. *Nat. Rev. Drug Discovery* **2007**, *6*, 721–733.
- (4) Melancon, B. J.; Hopkins, C. R.; Wood, M. R.; Emmitte, K. A.; Niswender, C. M.; Christopoulos, A.; Conn, P. J.; Lindsley, C. W. Allosteric modulation of 7 transmembrane spanning receptors: theory, practice and opportunities for CNS drug discovery. *J. Med. Chem.* **2012**, *55*, 1445–1464.
- (5) Conn, P. J.; Jones, C.; Lindsley, C. W. Subtype selective allosteric modulators of muscarinic receptors for the treatment of CNS disorders. *Trends Pharmacol. Sci.* **2009**, *30*, 148–156.
- (6) Bridges, T. M.; Kennedy, J. P.; Noetzel, M. J.; Breining, M. L.; Gentry, P. R.; Conn, P. J.; Lindsley, C. W. Chemical lead optimization of a pan G_q mAChR M₁, M₃, M₅ positive allosteric modulator (PAM) lead. Part II: Development of a potent and highly selective M₁ PAM. *Bioorg. Med. Chem. Lett.* **2010**, *20*, 1972–1975.
- (7) Byun, N. E.; Grannan, M.; Bubser, M.; Barry, R. L.; Thompson, A.; Rosanelli, J.; Gowrishankar, R.; Kelm, N. D.; Damon, S.; Bridges, T. M.; Melancon, B. J.; Tarr, J. C.; Brogan, J. T.; Avison, M. J.; Deutch, A. Y.; Wess, J.; Wood, M. R.; Lindsley, C. W.; Gore, J. C.; Conn, P. J.; Jones, C. K. Antipsychotic drug-like effects of the selective M₄ muscarinic acetylcholine receptor positive allosteric modulator VU0152100. *Neuropsychopharmacology* **2014**, *39*, 1578–1593.
- (8) Gentry, P. R.; Bridges, T. M.; Lamsal, A.; Vinson, P. N.; Smith, E.; Chase, P.; Hodder, P. S.; Engers, J. L.; Niswender, C. M.; Daniels, J. S.; Conn, P. J.; Wood, M. R.; Lindsley, C. W. Discovery of ML326: the first sub-micromolar, selective M₅ PAM. *Bioorg. Med. Chem. Lett.* **2013**, *23*, 2996–3000.
- (9) Gentry, P. R.; Kokubo, M.; Bridges, T. M.; Kett, N. R.; Harp, J. M.; Cho, H. P.; Smith, E.; Chase, P.; Hodder, P. S.; Niswender, C. M.; Daniels, J. S.; Conn, P. J.; Wood, M. R.; Lindsley, C. W. Discovery of the first M₅-selective and CNS penetrant negative allosteric modulator (NAM) of a muscarinic acetylcholine receptor: (S) 9b-(4-chlor-

ophenyl)-1-(3,4-difluorobenzoyl)-2,3-dihydro-1*H*-imidazo[2,1-*a*]-isoindol-5(9*bH*)one (ML375). *J. Med. Chem.* **2013**, *56*, 9351–9355.

(10) Thomsen, M.; Wortwein, G.; Fink-Jensen, A.; Woldbye, D. P. D.; Wess, J.; Caine, S. B. Decreased prepulse inhibition and increased sensitivity to muscarinic, but not dopaminergic drugs in *M*₅ muscarinic acetylcholine receptor knockout mice. *Psychopharmacology* **2007**, *192*, 97–110.

(11) Araya, R.; Noguchi, T.; Yuhki, M.; Kitamura, N.; Higuchi, M.; Saïdo, T. C.; Seki, K.; Itoharu, S.; Kawano, M.; Tanemura, K.; Takashima, A.; Yamada, K.; Kondoh, Y.; Kanno, I.; Wess, J.; Yamada, M. Loss of *M*₅ muscarinic acetylcholine receptors leads to cerebrovascular and neuronal abnormalities and cognitive deficits in mice. *Neurobiol. Dis.* **2006**, *24*, 334–344.

(12) Yamada, M.; Lamping, K. G.; Duttaroy, A.; Zhang, W.; Cui, Y.; Bymaster, F. P.; McKinzie, D. L.; Felder, C. C.; Deng, C.-X.; Faraci, F. M.; Wess, J. Cholinergic dilation of cerebral blood vessels is abolished in *M*₅ muscarinic acetylcholine receptor knockout mice. *Proc. Natl. Acad. Sci. U.S.A.* **2001**, *98*, 14096–14101.

(13) Kim, H. A.; Miller, A. A.; Drummond, G. R.; Thrift, A. G.; Arumugam, T. V.; Phan, T. G.; Srikanth, V. K.; Sobey, C. G. Vascular cognitive impairment and Alzheimer's disease: role of cerebral hypoperfusion and oxidative stress. *Naunyn-Schmiedeberg's Arch. Pharmacol.* **2012**, *385*, 953–959.

(14) For the MLPCN see <http://mli.nih.gov/mli/mlpcn/>. ML380 is an MLPCN probe and freely available upon request.

(15) Baell, J. B.; Holloway, G. A. New substructure filters for removal of pan assay interference compounds (PAINS) from screening libraries and for their exclusion in bioassays. *J. Med. Chem.* **2010**, *53*, 2719–2740.

(16) Gentry, P. R.; Kokubo, M.; Bridges, T. M.; Cho, H. P.; Smith, E.; Chase, P.; Hodder, P. S.; Utley, T. J.; Rajapakse, A.; Byers, F.; Niswender, C. M.; Morrison, R. D.; Daniels, J. S.; Wood, M. R.; Conn, P. J.; Lindsley, C. W. Discovery, synthesis and characterization of a highly mAChR selective *M*₅ orthosteric antagonist, VU0488130 (ML381): a novel molecular probe. *ChemMedChem* **2014**, *9*, 1677–1682.

(17) See Supporting Information for full details.